An Assessment of Short-medium Term Interventions Using CAESAR-Lisflood in a Post-earthquake Mountainous Area

Di Wang[1,2,3], Ming Wang[1], Kai Liu[1], Jun Xie[1]

[1]School of National Safety and Emergency Management, Beijing Normal University, Beijing, China.

[2]Academy of Disaster Reduction and Emergency Management, Beijing Normal University, Beijing, China.

[3]Faculty of Geographical Science, Beijing Normal University, Beijing, China.

Correspondence to: Ming Wang (wangming@bnu.edu.cn)

Abstract. The 2008 Wenchuan earthquake rapidly triggered local geomorphic changes, shifting abundant material through exogenic processes and creating vast amounts of loose material. The substantial material dynamics increased the risks of geo-hazards (flash floods, landslides, and debris flows) induced by extreme precipitation in the area. Intervention measures such as dams, levees, and vegetation revetments have been constructed in specified sites to reduce sediment transport, thus mitigating the risk of ensuing geo-hazards.

This study assessed the effects of various interventions, incorporated with multiple facilities, on post-earthquake fragile mountains in the short-medium term. Taking the Xingping valley as an example, we used CAESAR-Lisflood software, a two-dimensional landscape evolution model, to simulate three scenarios: unprotected landscapes, present protected landscapes, and enhanced protected landscapes between 2011 and 2013. We defined two indicators to assess the intervention effects of the three scenarios by comparing the geomorphic changes and sediment yields.

The results show that the mitigation facilities are effective, especially engineering efforts cooperating with vegetation revetments in the upstream area. The spatial patterns of erosion and deposition change considerably due to the intervention measures. Additionally, the effectiveness of each intervention scenario shows a gradual decline over time caused directly by the reduction in the reservoir's capacity. The enhanced scenario performs better than the present one, with a smaller downward trend. The simulation results assess the ability and effectiveness of cooperated control measures and will support optimum mitigation strategies.

1 Introduction

Strong earthquakes can trigger co-seismic landslides, discontinuously crack mountains, and thus increase weak structural planes (Huang, 2009) by weathering and erosion. Consequently, material shifted from coseismal landslides and attendant mass failures caused by weakened slopes modify mountain landscapes by various surface processes for days, years, and millennia (Fan et al., 2020). The 2008 Wenchuan Ms 8.0 (the surface-wave magnitude, which is the logarithm of the maximum amplitude of the ground motion of the surface waves with a wave period of 20 seconds) earthquake has been influencing towns and other infrastructure in the affected area. Many studies have mapped the landslides triggered by this devastating earthquake. One study, Gorum et al. (2011), performed an extensive landslide interpretation using a large set of high-resolution optical images and mapped nearly 60,000 individual landslides, all impacting an area of 600 m^2 or more. Another study, Xu et al. (2014), delineated 197,481 landslides formed by polygons, centroids, and top points compiled from visual image interpretation. To estimate the threat of loose material in subsequent sediment disasters caused by landslides, some research has attempted to measure the volume of deposited material based on field surveys and assumptions. For example, Huang and Fan (2013) estimated that 400 million m^3 of material was deposited in heavily affected areas by assuming that the material was deposited on steep slopes with angles larger than 30° and a catchment area of more than 0.1 km^2. An approximate 2,793 million m^3 of sediment was calculated by Chen et al. (2009) using different deposited depth settings in different buffer zones of the Longmenshan central fault. In summary, a tremendous amount of loose material accumulated in the gullies and hillslopes which became available for erosion and other exogenic processes for years to come. As a result, mitigation in the Wenchuan earthquake-stricken area is still ongoing.

Structural mitigation measures have been developed in the affected areas depending on the different site conditions and other technical and economic feasibilities. For example, ecological mitigation, such as vegetation revetments, was conducted to stabilise the source area in hillslopes (Cui and Lin, 2013; Forbes and Broadhead, 2013; Stokes et al., 2014), and check dams were used widely to intercept upriver sediment (Yang et al., 2021; Marchi et al., 2019). And lateral walls and levees which are longitudinal structures (Marchi et al., 2019), can be built to protect infrastructure in mountain watersheds with relatively higher sediment runoff into main streams.

Although comprehensive mitigation measures were performed at potentially dangerous sites, disasters still occurred due to rough terrain, vague source material, intensive precipitation, and relatively low-cost mitigation measures (Yu et al., 2010; Cui et al., 2013). Therefore, understanding the effectiveness of intervention measures is crucial for mitigation strategies. Some studies focus on establishing post-evaluation effectiveness index systems that are not supported by sufficient practices (Zhang and Liang, 2005; Wang et al., 2015). Some researchers compare the changes before and after intervention measures by recording long-term on-site measurements, which face the challenges of needing a great deal of time, energy and financing (Zhou et al., 2012; Chen et al., 2013). Recent research has compared disaster characteristics before and after mitigation actions, which are quickly obtained from numerical simulations (Cong et al., 2019; He et al., 2022). Nevertheless, these disaster characteristics ignore the long-term effects of earthquakes on geomorphic changes (longer than the duration of a single event). Therefore, the short-medium term (from the duration of a single event to decades after) and spatial geomorphic changes obtained from simulations provide more details to interpret engineering measures in notable locations, even in locations inaccessible to humans.

CAESAR-Lisflood (C-L), which is based on the cellular automata (CA) framework (Coulthard et al., 2013), has powerful spatial modelling and computing capabilities to simulate complex dynamic systems (Batty and Xie, 1997; Couclelis, 1997; Coulthard et al., 2002). The model enables the study of many earth system interactions under different geo-environmental. Representation of deposition and erosion within C-L is used widely in rehabilitation planning and soil erosion predictions in post-mining landforms (Saynor et al., 2019; Hancock et al., 2017; J.B.C. Lowry et al., 2019; Thomson and Chandler, 2019; Slingerland et al., 2019) as well as channel evolution and sedimentary budget planning for dam settings (Poeppl et al., 2019; Gioia and Schiattarella, 2020; Ramirez et al., 2020, 2022). In addition, there have been a series of studies in mountainous area involving secondary geo-hazard driving factors (Li et al., 2018; Wang et al., 2014b) and vegetation recovery (Zhang et al., 2018). One study, Li et al. (2020) and Xie et al. (2018) used C-L with different rainfall and future climate change scenarios to interpret the landscape evolution after the Wenchuan earthquake. The methods and parameter values used in the above research helped promote this model's application in other study areas.

In this study, hourly rainfall data over three years were generated by daily downscaling to capture extreme events. Based on the input data, we simulated and compared the geomorphic changes and sediment yield in three scenarios that varied in their mitigation compositions and intensities in the catchment. The objectives were 1) to assess the effectiveness of a set of mitigation facilities to reduce sediment transport, 2) to analyse the role of each facility on geomorphic changes, and 3) to determine the influence of vegetation on catchment erosion.

2 Study area

2.1 Regional characteristics

The study area was the Xingping valley in north-eastern Sichuan Province, the left branch of the Shikan River (a tributary of the Fu River) (Fig. 1). There are nearly two hundred households scattered among more than five villages in the catchment. The topography of the catchment is rugged, with an elevation between 800 and 3036 m and an area of approximately 14 km^2. The catchment is characterised by a high longitudinal gradient (~ 120‰) and more than ten small V-shaped branch gullies. The length from the northeast to the southwest is 5,770 m, and the width is 4,150 m in the perpendicular direction. The region has a humid temperate climate with a mean annual temperature of 14.7℃. The mean annual precipitation is 807.6 mm, mainly between May and September. The steep terrain and short-term heavy rainfall dominate ephemeral streams in this area.

The local basement rocks are mainly metamorphic sandstones, sandy slate, crystalline limestone, and phyllite of the Triassic Xikang Group (T_{3xk}) and Silurian Maoxian Group (S_{mx}), which are easily worn away by quick weathering in static processes after disturbs caused from strong earthquakes. Consequently, the Wenchuan earthquake, with a Modified Mercalli Intensity scale of X, made this area one of the most severely affected locations (Wang et al., 2014a) and produced 10^6 m^3 loose material by triggering landslides and subsequent weathering in Mayuanzi, Zhengjiashan, and Wujiaping (Fig. 1)(Guo et al., 2018).

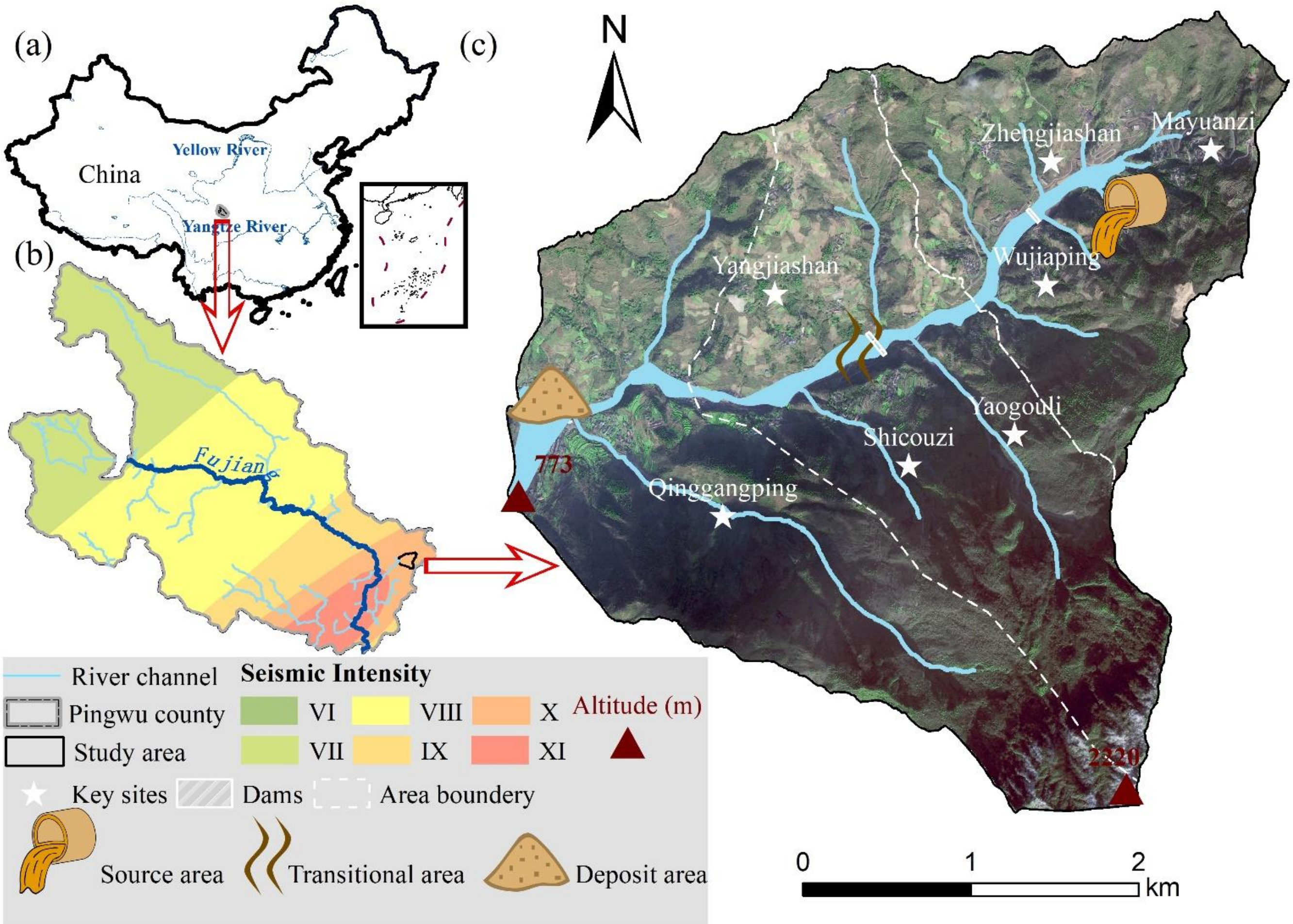

Figure 1: An overview of the study area. (a) The location of the study area; (b) A seismic intensity map of the Wenchuan earthquake within Pingwu County; (c) A schematic image of the study area.

2.2 Historical hazards and intervention measures

Six debris flow-flash flood disaster chain groups have been found in the Xingping valley over the decade after the earthquake. Based on the published work of SKLGP (State Key Laboratory of Geohazard Prevention and Geoenvironment Protection) and the local states' geological survey before 2018 and our biannual field surveys since 2012, we catalogued the time of occurrence, total rainfall of each event, and corresponding disaster details (Table S1). The massive sediment was transported quickly after the devastating earthquake in 2008 and 2009, and the extreme rainfall in 2013 and 2018 triggered the deposition of extensive loose material in the channel. Considering the landslide processes, we divided the study area into three regions: the source area, the transitional area, and the deposit area. The white dashed lines in Fig. 1c, indicate that the loose solid material can easily be transported from the source area to the deposit area through the transitional zone.

An engineering control project was constructed to intercept the upriver material in October 2010. The project included two check dams, one in the upper source area and the other in the transitional zone (Feng et al., 2017) (Fig. 1c). The upper dam has a storage capacity of 5.78×10^4 m^3 and a height of 10.0 m. The transitional area dam has a storage capacity of 7.2×10^4 m^3 and a height of 9.0 m. With the reservoirs gradually filling with deposits, the first dredging work was subsequently performed in 2013. Nearly three years later, the storage capacity behind the upper dam remained at 50% in 2016, while the transitional area dam could no longer retain sediment.

3 Materials and Methods

In this study, we examined the intervention effectiveness through the morphological response and sediment yield in the Xingping valley, which was simulated using the C-L model. The research entailed four main steps: 1) setting three scenarios with different intervention compositions, 2) preprocessing the model input data, including three groups of DEMs, the rainfall data, and the m value of the C-L, 3) calibration of the hydrological component, and 4) simulating landscape changes and analysing the intervention effectiveness in 2011-2013.

3.1 Scenario settings

The abundant source material triggered by landslides should be controlled to prevent the threat of disasters downstream. Therefore, we designed three scenarios by incorporating engineering and biological measures referenced to current facilities to assess the effectiveness of intervention measures. Scenario UP: Unprotected landscapes meant the sediment would be transported without anthropogenic intervention. Scenario PP: Present protected landscapes implied that only the present two check dams trapped sediment in 2011-2013 without dredging work over the period (see Section 2.2). Scenario EP: Enhanced protected landscapes emphasised the addition of vegetation revetments in the source area and levees in the deposit area based on the two check dams in Scenario PP.

Figure 1c shows the locations of the existing two check dams in both Scenario PP and Scenario EP. We determined the placements of additional facilities in Scenario EP according to the field survey, which demonstrated that the continuous supply of sediment was mainly from the source area. Therefore, vegetation revetments such as tree planting would be carried out upstream to prevent erosion by stabilising the topsoil and enhancing the soil's infiltration capacity via roots (Lan et al., 2020). Considering the damage caused by flash floods to the residential area downstream, the levees (see Fig. S1 and Section 3.2.2) are artificial barriers to protect agricultural land and buildings, which help to prevent water and sediment from overflowing and flooding surrounding areas. Table 1 shows the scenario descriptions, initial model conditions and input rainfall series. The details about the model input data are introduced below.

Table 1: Scenario settings

Scenario	Descriptions	Period	DEM (10 m)	Rainfall data
UP	no anthropogenic intervention	2011-2013 (3 years)	UP DEM UP bedDEM	downscaled hourly precipitation over the period (lumped)
PP	the present two check dams upstream without dredging work		PP DEM PP bedDEM	
EP	additional vegetation revetments in the source area and levees in the deposit area based on Scenario PP		EP DEM EP bedDEM	downscaled hourly precipitation over the period (spilt)

3.2 CAESAR-Lisflood

The C-L integrated the Lisflood-FP 2D hydrodynamic flow model (Bates et al., 2010) with the CAESAR landscape evolution model (LEM) (Coulthard et al., 2002; Van De Wiel et al., 2007), which is described in detail by Coulthard et al. (2013). The catchment mode of C-L was applied in this study, in which the surface digital elevation model (DEM), the bedrock DEM, the grain size distribution, and a rainfall time series are required to simulate the sediment transport and geomorphic changes. There are four primary modules within C-L operated as follows:

(1) a hydrological module generates surface runoff from rainfall input using an adaptation of TOPMODEL (topography-based hydrological model) (Beven and Kirkby, 1979),

(2) a hydrodynamic flow routing module based on the Lisflood-FP method (Bates et al., 2010) which calculates the flow depths and velocities,

(3) an erosion and deposition module uses hydrodynamic results to drive fluvial erosion by either the Einstein (1950) or the Wilcock et al. (2003) equations applied to each sediment fraction over nine different grain sizes,

(4) and a slope model of the movement of material from the hillslope to the fluvial system by considering both the mass movement when a critical slope threshold is exceeded and soil creep processes whereby sediment flux is linearly proportional to the surface slope.

The C-L model updates variable values stored in square grid cells at intervals, such as DEM, grain size and proportion data, water depth, and velocity. For the three scenarios, the initial conditions, such as DEMs and bedrock DEMs, the rainfall data, and the m values, were preprocessed as follows.

3.2.1 The surface and bedrock digital elevation models

To clearly describe the control process, especially the two dams and levees in the catchment, we unified grid cell scales to 10 m for all input data of the C-L. The GlobalDEM product with a 10 m × 10 m resolution and 5 m (absolute) vertical accuracy were used to form three types of initial DEMs (UP DEM, PP DEM, and EP DEM). Before rebuilding the initial DEMs, we filled the sinks of the original GlobalDEM based on the Environmental Systems Research Institute's (ESRI's) ArcMap (ArcGIS, 10.8) to eliminate the 'walls' and the 'depressions' in the cells and thus avoided intense erosion or deposition in the early run time. Then, the non-sink DEM was used as the surface DEM in Scenario UP (UP DEM) without any facilities. According to the engineering control project described in Section 3.2.2, the surface DEM of Scenario PP (PP DEM) included the dams by raising the grid cell elevations by 10 m for the dam in the upper stream and 9 m for the dam in the transitional area.Similarly, the surface DEM in Scenario EP (EP DEM) included the dams in the PP DEM. In addition, two levees were produced by raising the grid cell elevation by 2 m, representing at selected locations. For scenario EP, the placement and setting of the vegetation revetments are introduced in Section 3.2.2.

The spatial heterogeneity of the source material (Fig. 1c) indicates the discrepancy in the erodible thickness, which equals the difference between the surface DEM (DEM) and the bedrock DEM (bedDEM). We divided the study area into five regions according to the erodible thickness (Fig. S1) by checking the relative elevation of the foundations of buildings, the exposed bedrock, and the deposition depth of landslides to ground level. The average thicknesses of upstream low- and high-altitude areas were set to 10 m and 3 m, respectively, and the thickness of the erodible layer in the downstream area was set to 3 m. For the river channel and outlet, as there would be a large amount of deposition, the thickness of erodible sediment was set to 5 m and 4 m, respectively. As the dams in Scenario PP and the levees in Scenario EP were non-erosive concrete, we set the erodible thickness of these features to 0 m. Eventually, the DEM data were formatted to ASCII raster data as required by C-L. The divided regions varied in erodible thickness, the placement of additional levees and vegetable revetments in Scenario EP, and the generation process of DEMs and bedDEMs are shown in Fig. S1.

3.2.2 Vegetation settings

Another parameter required in each scenario simulation was the m value of the hydrological model (TOPMODEL) within C-L, which controls an exponential decline in transmissivity with depth (Beven, 1995, 1997) and influences the peak and duration of the hydrograph in response to rainfall. The m value effectively imitates the effect of vegetation on the movement and storage of water within the soil. The lower the m value is, the lower the vegetation coverage, and the higher the flash flood peak and the shorter the duration of the flood hydrograph is reflected (Coulthard et al., 2002). The m value is usually determined by the land cover (e.g., 0.02 for forests and 0.005 for grasslands) (Coulthard and Wiel, Van De J., 2017). In our study, we set the m value as 0.008 in our smaller catchment (14 km^2) in Scenarios UP and PP, which resembles the m value of farmland covered with lower vegetation coverage in the same catchment studied by Xie et al. (2018) and Li et al. (2018). As mentioned earlier, the upstream-low elevation area covered by the biological measures in the EP scenario was assigned a higher m value of 0.02. This m value was calibrated by the more extensive catchment containing our study area in the flood event of 2013 (Xie et al., 2018).

3.2.3 The rainfall data

In this research, we compared three scenarios by matching precipitation data between 2011 and 2013, as mentioned in Section 3.1. The source data of precipitation in 2011-2013 (Fig. 2a) were obtained from the China Meteorological Administration (http://data.cma.cn) with daily temporal resolution. The intensity and frequency of extreme rainfall events affect patterns of erosion and deposition (Coulthard et al., 2012b; Coulthard and Skinner, 2016). Therefore, we used the stochastic downscaling method to generate hourly data to better capture the hydrological events introduced by Li et al. (2020) and Lee and Jeong (2014). The referenced hourly precipitation was observed from the pluviometer located 20 km from the study area in 2016 (Fig. 2b), with an annual total precipitation of 684 mm. The observed rainfall in 2016 was characterised by (1) hourly precipitation between 1.1 mm and 35.4 mm and (2) the maximum and average durations of rainfall events as 24 h and 2.8 h, respectively. The main processes of the downscaling method are as follows:

- extracting the hourly rainfall of specific days in 2016 closest to the daily rainfall in 2011-2013 through the threshold setting and producing the genetic operators using the extracted hourly rainfall dataset;
- mixing the genetic operators by an algorithm (Goldberg, 1989) composed of reproduction, crossover and mutation and repeating until the distance between the sum of hourly rainfall and the actual daily rainfall was less than the set threshold;
- normalising the hourly precipitation to keep the daily rainfall value unchanged.

Figure 2c shows the downscaled rainfall series between 2011 and 2013. The downscaled hourly rainfall better captured the hydrological events at an hourly scale compared to the hourly mean rain (5.27 mm) on the day with extreme rainfall (126.5 mm), which was far from the actual situation. Corresponding to the m value settings, the input of generated hourly precipitation was catchment lumped in Scenario UP and Scenario PP and divided into two separate but identical rainfall events in Scenario EP.

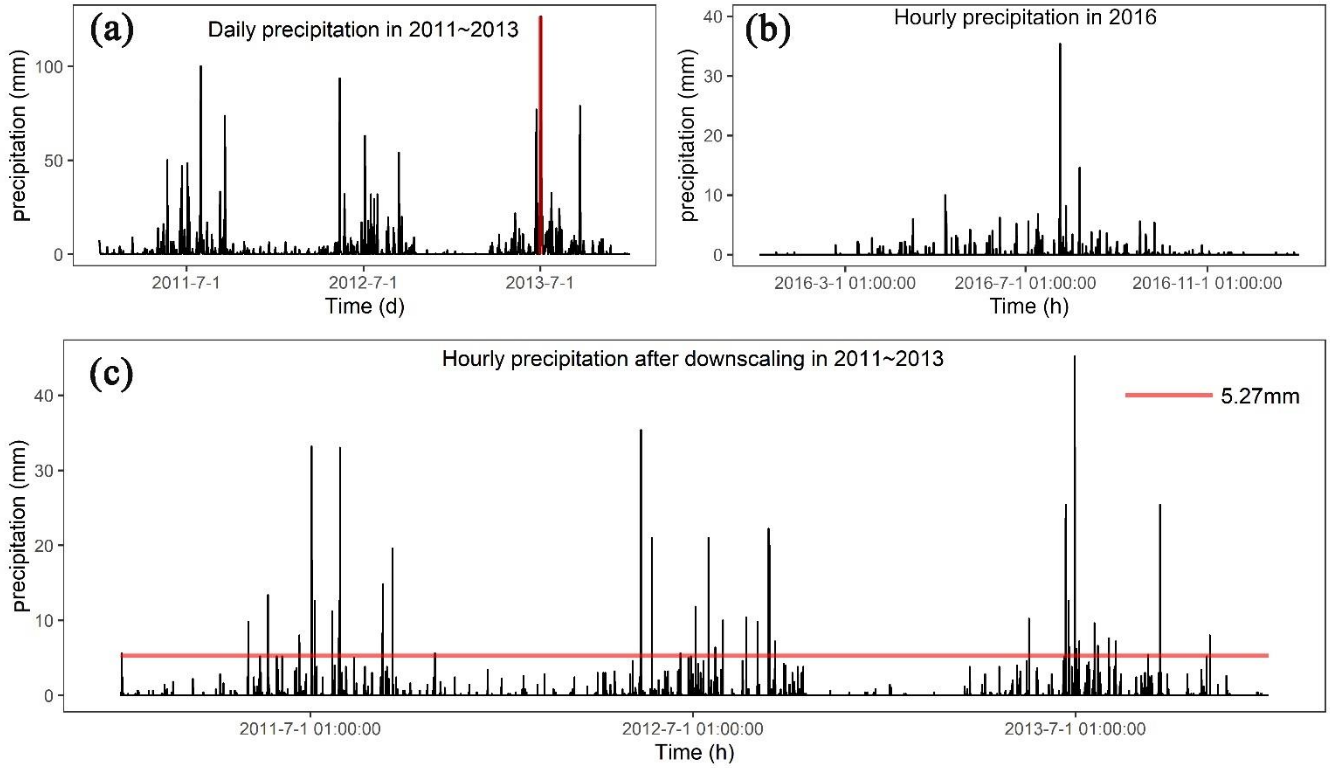

Figure 2: (a) Daily precipitation in 2011-2013 (the red vertical line indicates the maximum daily precipitation of 126.5 mm); (b) Hourly precipitation in 2016; (c) Downscaled hourly precipitation in 2011-2013 (the red horizontal line indicates the hourly mean precipitation of 5.27 mm on the day with the maximum precipitation marked in (a)).

3.2.4 Other parameters

The C-L model is sensitive to a set of input data introduced by Skinner et al. (2018) for a catchment with a grid cell size of 10 m, such as the sediment transport formula, slope failure threshold, and grain size set. The grain size distribution of sediment was derived from samplings at 14 representative locations in the same study basin by Xie et al. (2018). Given the grain size distribution in this study, the Wilcock and Crowe formula was selected as the sediment transport rule, which was developed from flume experiments using five different sand-gravel mixtures with grain sizes ranging between 0.5 and 64 mm (Wilcock et al., 2003). Considering the steep slopes on either side of deep gullies, a higher slope failure threshold was determined to replicate the geomorphic changes between 2011 and 2013. Additionally, we found that the probability of shallow landslides increased from 20° to 50° in slope gradients between 2011 and 2013 (Li et al., 2018). The slope angle was derived from the DEM with a 30 m spatial resolution, which caused a lower slope angle than that with a 10 m resolution. As such, we set the slope angle as 60°, which is lower than the 65° used in a scenario without landslides (Xie et al., 2022) and higher than 50°. Some parameters were determined by repeated experiments, such as the minimum Q value, and the other input values were referred to default values recommended by the developers (such as the maximum erosion limit in the erosion/deposition module and the vegetation critical shear stress) in https://sourceforge.net/p/caesar-lisflood/wiki/Home/. Table S2 in the supplemental material presents the model parameters of C-L used in this study.

3.2.5 Model calibration

Considering the ungauged basins before 2015, we replicated the flash flood event in July 2018 using C-L simulations to calibrate the hydrological components. Based on Scenario PP (with two checking dams), we used the two-week hourly precipitation of July 2018 as the input (Fig. S2a), which was recorded by a rain gauge located 2.5 km away from the catchment (Fig. S2b). The simulation results (Fig. S2c and Fig. S2d) showed an erosion map and a maximum water depth map in Scenario PP on July 15, 2018. We selected three locations to compare the deposition and inundation in the simulation results with satellite images and photos (Fig. S3). Additionally, the simulated sediment thickness and water depth were close to those measured from pictures, which indicated that the flash flood event was well replicated by the C-L using the input data.

3.3 Output analysis

The C-L model outputs of each scenario include hourly water and sediment discharge at the basin outlet and the difference between DEMs at a specified time and initial DEMs (EleDiffs). We validated the model outputs by comparing the hourly discharge and EleDiffs reflecting the depth of sediment deposition or erosion (> 0.1 m: deposition, < -0.1 m: erosion) with field survey materials. The overall temporal and spatial geomorphic changes reflected by EleDiffs under three different scenarios were used to assess the geomorphic response to interventions. To explore the geomorphic response to various control measures, we focused on the notable sites where the checking dams, levees, and vegetation revetments would be located and recorded the depth of accumulating sediment behind the two dams. To further explore the spatial heterogeneity, we compared the volumes of deposition and erosion among three divided regions, including the source area, the transitional area, and the deposit area.

Based on the visual analysis and quantitative results, we defined two formulae to assess the effectiveness of the intervention. The conservation ability (*Ca*, Eq. (3)) was calculated based on variables in the sediment balance system (Fig. 3). The sediment volume of deposited sediment (D_n) and input sediment from the upper connected region (I_n) is equal to that of the eroded material (E_n) and the output sediment to the next part (O_n) over the same period (Eq. (1), Eq. (2)) in the system. A higher value of *Ca* in a specific region and scenario indicates a more effective control system.

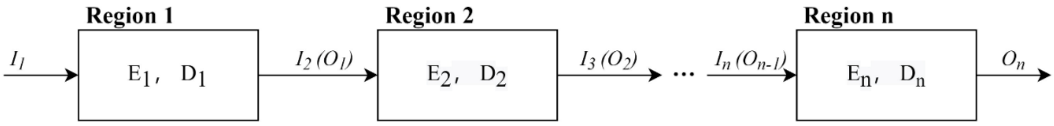

Figure 3: The sediment balance system in the study area (the Region *n* indicates the source area, transitional area, and deposit area)

$$I_n = \sum_{2}^{n} E_{n-1} - \sum_{2}^{n} D_{n-1}, \tag{1}$$

$$I_n + E_n = O_n + D_n, \tag{2}$$

$$Ca = \frac{D_n}{I_n + E_n} \tag{3}$$

where *n* is the region number of the source area (=1), transitional area (=2), and deposit area (=3).

Additionally, we designed the relative efficiency (*Re*, Eq. (4)) to depict the efficiency of intervention measures in Scenario PP and EP in sediment loss, with the comparison to Scenario UP.

$$Re_{PP/EP,i} = \frac{Q_{UP,i} - Q_{PP/EP,i}}{Q_{UP,i}} \tag{4}$$

where i is the sequence of the day; Q_{UP} is the daily sediment yield measured at the catchment outlet in Scenario UP, and $Q_{PP/EP}$ is the same data in Scenario PP or Scenario EP of day i; and $Re_{PP/EP}$ is the daily relative effectiveness of control measures in Scenario PP or Scenario EP.

4. Results

4.1 Model verification

Figure 4 shows the input rainfall data and modelled discharge hydrograph between 2011 and 2013 (Fig. 4a). The comparison of simulated mean discharge in April through July and the whole year with field survey materials in the two locations are also presented (Fig. 4b, c). Concerning the discharge hydrograph, the peak discharges (63.7, 54.9, and 50.3 m^3/s) correspond well with the peak rainfall intensities (31, 19.7 and 15 mm). The modelled water discharge from March to May in location A is slightly larger than the measured value reported by Feng et al. (2017). Additionally, an average annual discharge of 10.04 m^3/s in location A is lower than that of 12.80 m^3/s in the catchment outlet (location B), which has an area approximately three times the size of the study area.

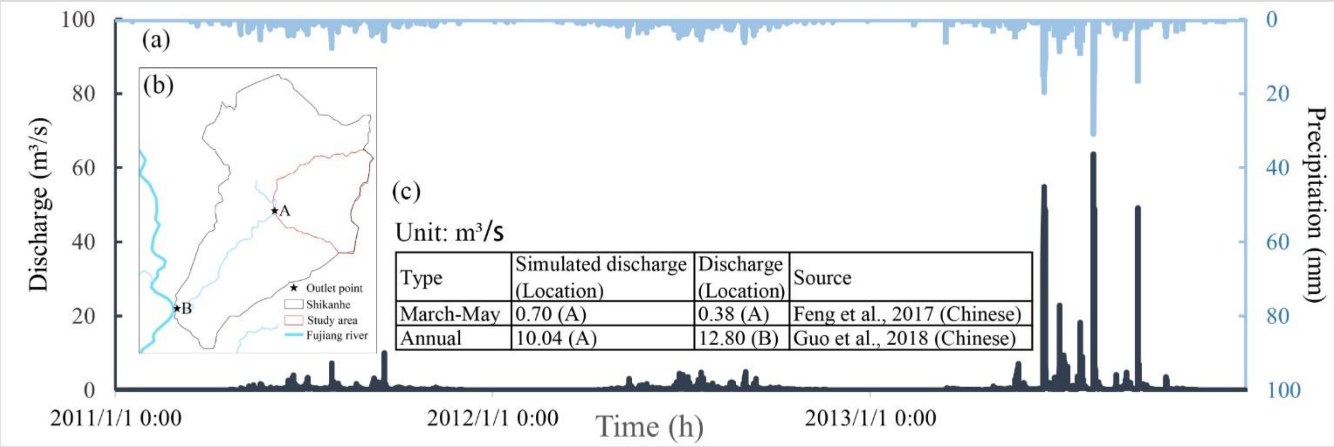

Figure 4: The input and output of the hydrograph. (a) The input hourly precipitation and simulated discharge in 2011-2013 in Scenario PP; (b) The locations of the specified outlet points; (c) A comparison of the simulated average discharge to the recorded discharge.

Typical cross-sections are generated (Fig. 5) based on the replicated landscape changes in Scenario PP. The first site is located on the upriver road, which is eroded at a depth of 5.7 m according to the simulation results, while the photo shows a depth of no less than 4.0 m without an apparent eroded base. The cross-section #2 and the site photo of the gully depict that the eroded depth is approximately 1.0 m. Meanwhile, a clear sediment boundary is found in the building located at the deposited area (# 3), indicating a slightly lower deposition depth than the model predicted.

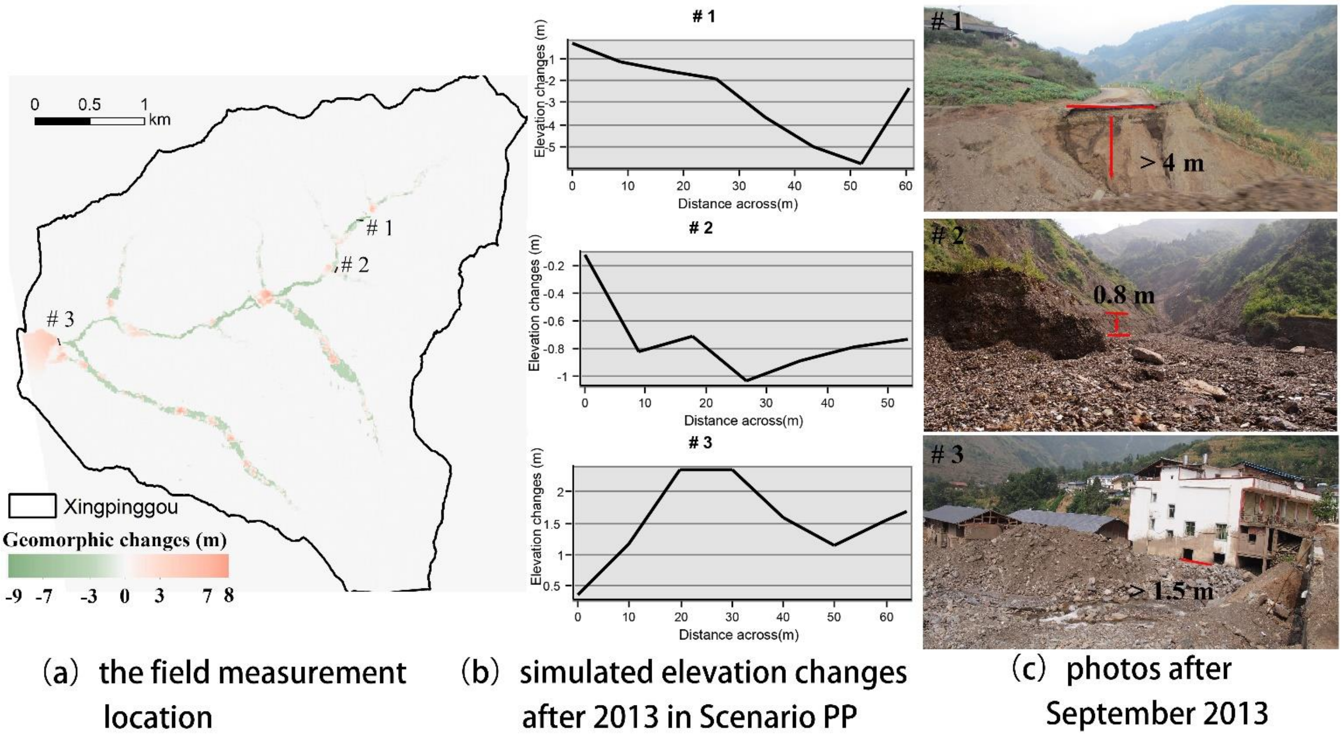

Figure 5: The comparison of cross-sections from the simulation results to the field measurements after 2013 in Scenario PP.

4.2 Overall geomorphic changes

Figure 6a compares the three annual landscape changes in each scenario, which are classified into nine categories by natural breaks for EleDiffs: extreme erosion (<-7 m), heavy erosion (-7--3 m), moderate erosion (-3--1 m), light erosion (1-0.1 m), micro change (-0.1-0.1 m), light deposition (0.1-1 m), moderate deposition (1-3 m), heavy deposition (3-7 m), and extreme deposition (>7 m). A similar spatial pattern of erosion is observed in all three scenarios. More specifically, erosion mainly emerges in the main channel and the branch valleys, among which the left branches are more pronounced. In contrast, the depositional zone appears to vary in the three scenarios, especially in the area behind the two dams shown in Scenarios PP and EP.

The total area of affected grid cells representing erosion and deposition for three scenarios are calculated to compare the damages (Figure 6b). The affected area in Scenario UP is approximately 0.76 km^2 (5.4% of the total catchment), which is larger than that in Scenario PP (0.70 km^2, 5.0% of the whole catchment), and the affected area decreases to 0.61 km^2 (4.4% of the total catchment) in Scenario EP. The total area of erosion and deposition decreases gradually with more controlling measures established in this study.

Figure 6c compares the extent of geomorphic changes in three situations using the ranges that varied in depth. The erosion area of the light one and moderate one is greater than the extreme and heavy erosion area for all three scenarios. The zone of each erosion degree in UP is more extensive than that in PP, followed by that in EP. In addition, the greater the deposition depth is, the smaller the deposition covers. In particular, the extreme deposition area is greater than the area of heavy deposition in the UP scenario. Further analysis shows that extreme, moderate, and light deposition area decrease in the order of UP, PP, and EP. The heavy deposition area shows the opposite trend, mainly attributed to the checking dams and vegetation revetments.

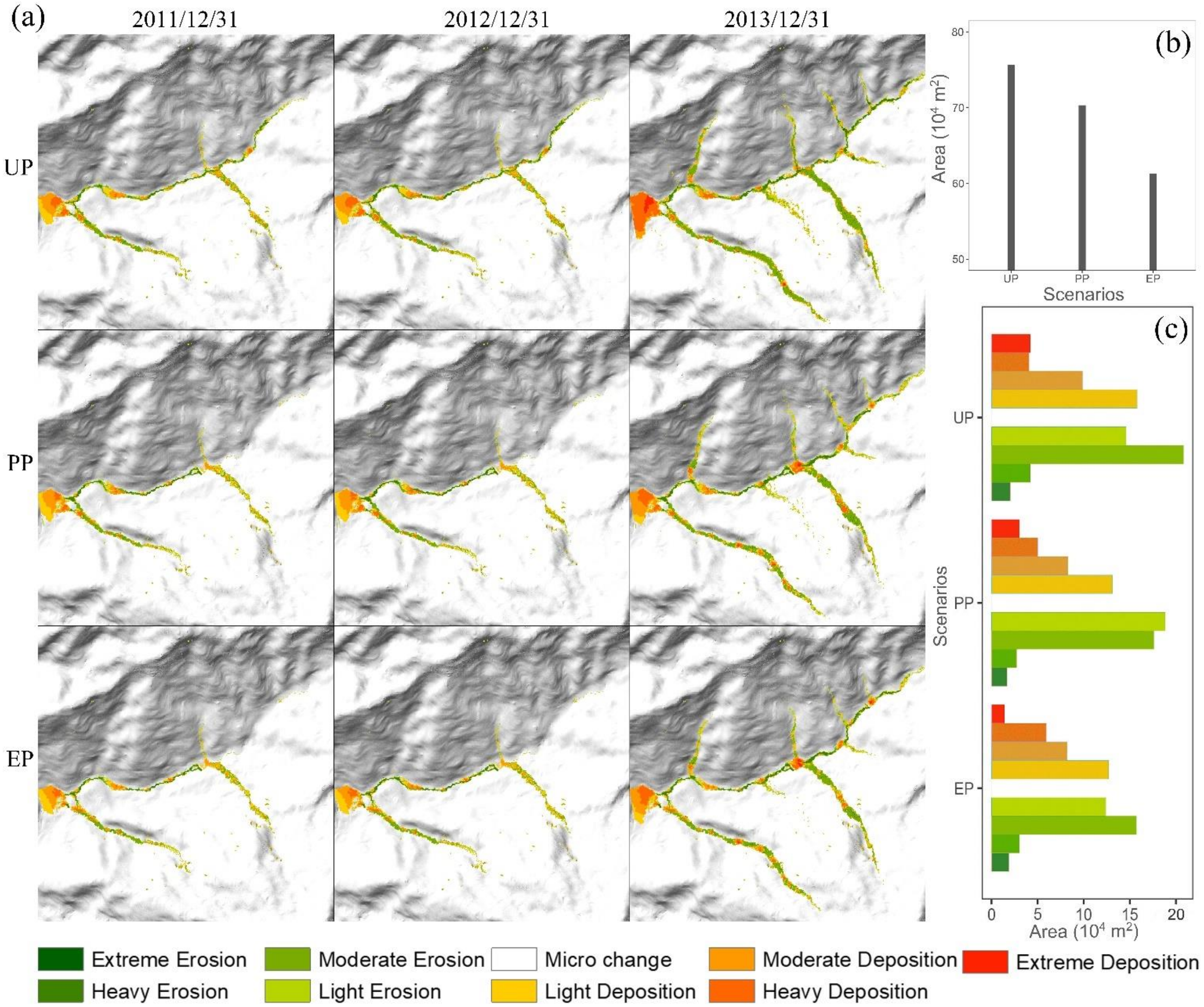

Figure 6: (a) Simulated geomorphic changes over time for the three scenarios; (b) The affected area of deposition and erosion for the three scenarios; (c) The columnar distribution of different erosion and deposition levels.

4.3 Details of key locations

As shown in Fig .7, the controlling measures and surroundings for the three scenarios are further investigated. Behind the two dams upriver in Scenarios PP and EP, the evident orange clusters indicate deposition. In contrast, these locations are dominated by erosion, shown in green in scenario UP. Further analysis of the sediment depth shown in Fig. 8 shows that the deposited depth behind the dams in Scenario EP is lower than that in Scenario PP. Additionally, in Scenario PP, sediment trapped by dam 1 is less than that of dam 2, but both have deposition thicknesses of more than 10 m, which exceed the dams' heights (dam 1's height is 10 m, dam 2's height is 9 m). For the simulation results in Scenario EP, the values of deposition depth behind the two dams are nearly 8 m, which is lower than the dams' heights.

The additional biological protection measure alters the material produced from the upriver tributary gullies. A sediment volume of 14.4×10^4 m^3 is transported from the biological protection area in the EP scenario (solid lines in Fig. 7). A total of 27.1×10^4 m^3 and 16.9×10^4 m^3 of loose material are produced in the same region without biological protection in Scenarios UP and PP, respectively. The vegetation revetment enhances sediment conservation based on the role of dam 1. Compared with the deposition in UP and PP without levees in the downriver area (shown in the bottom row of Fig. 7), the levees in EP block debris in the bend of the channel and play an essential role in protecting the residents and cultivated land behind the levees.

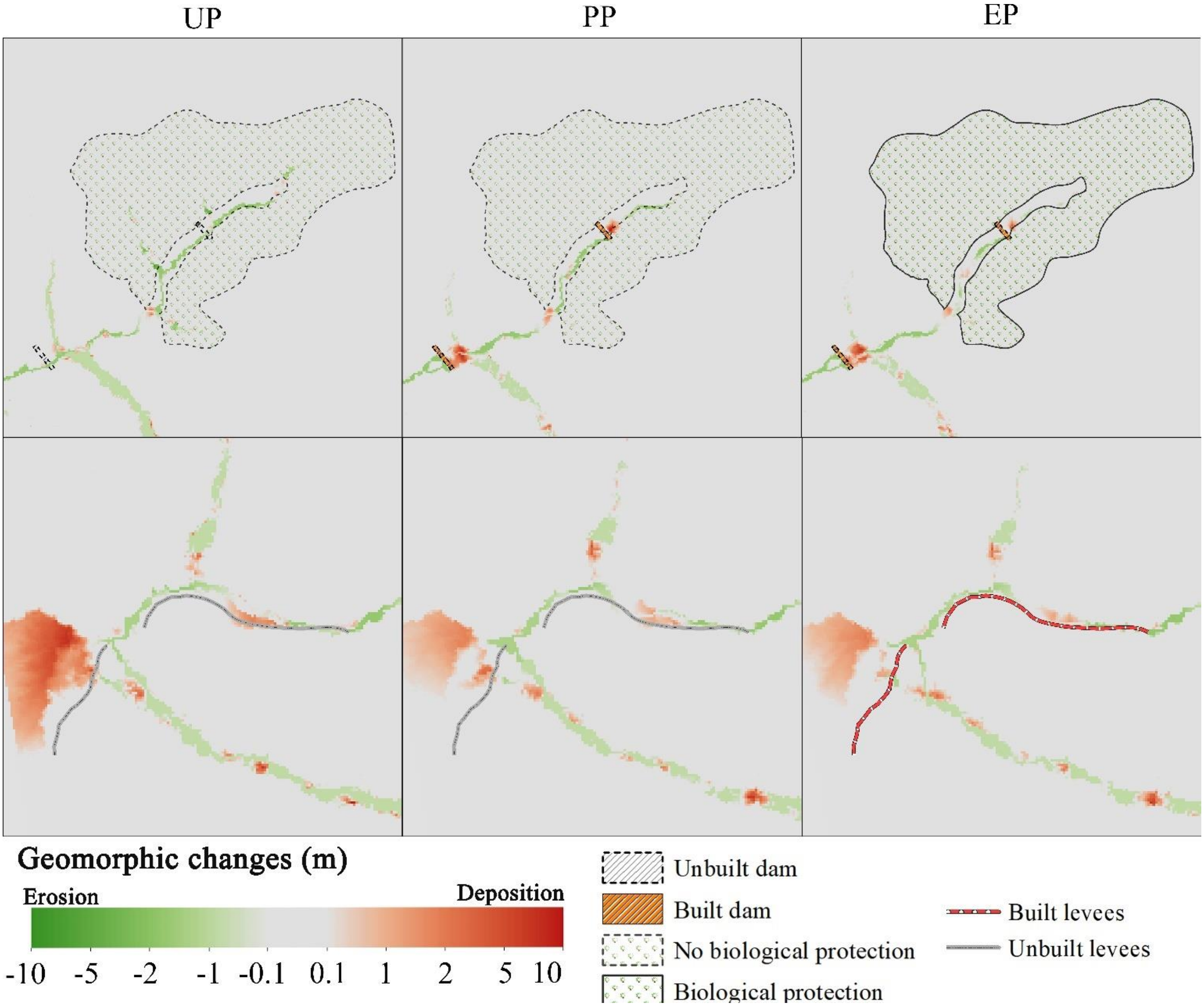

Figure 7: Geomorphic changes at key locations of the simulation results for the UP, PP, and EP scenarios. The top row is the upriver extent containing dam 1, dam 2 and the vegetation revetment. The bottom row is the downriver extent containing levees.

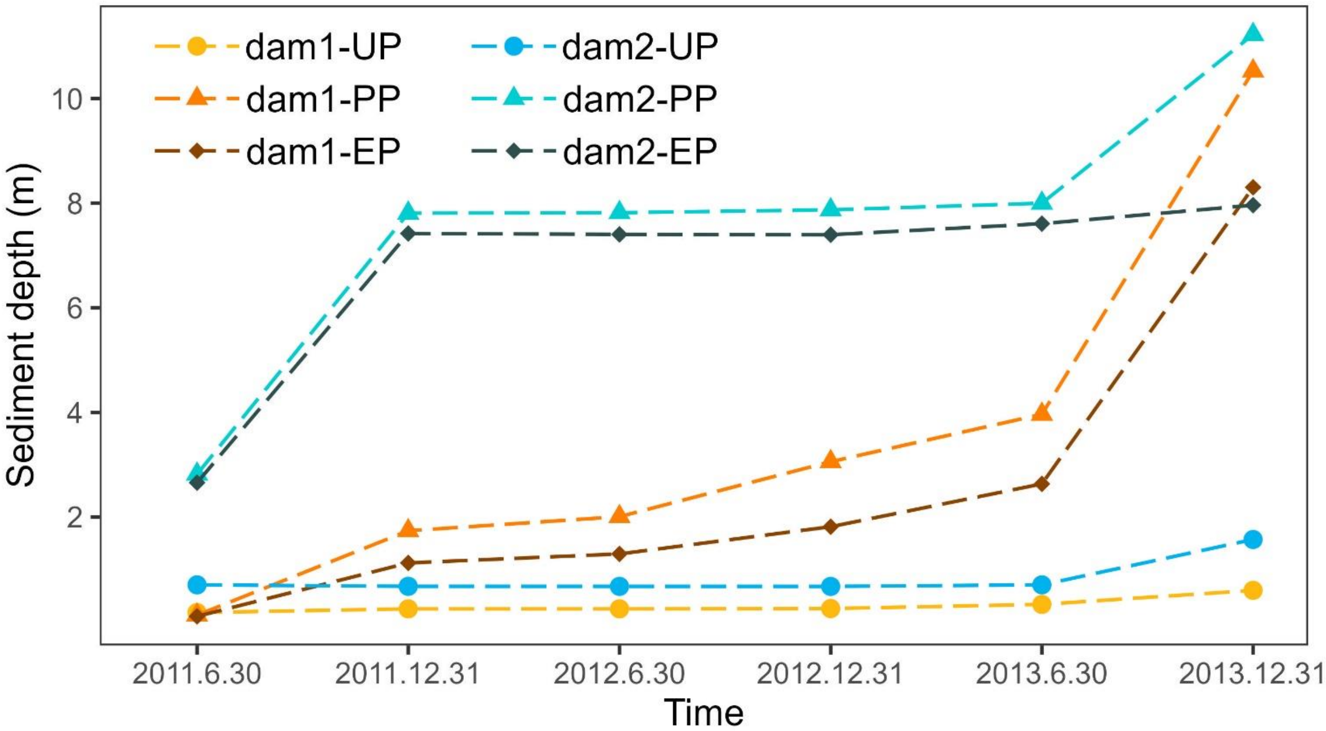

Figure 8: The depth of deposited sediment in the dams' placements.

4.4 Effectiveness assessment of the intervention measures

Figure 9 shows the erosion and deposition volumes in the source, transitional, and deposit areas and compares the conservation ability (*Ca*) in each scenario. For all three scenarios, the deposition volume in the source area is less than that in the transitional area, and the largest amount of sediment is accumulated in the deposit area. Regarding the eroded sediment, the largest volume is in the transitional area, followed by the transitional area, and the source area presents the lowest volume. Moreover, sediment transport is best controlled in the deposit area and worst contained in the source area under any intervention conditions. Compared with the *Ca* of the source area in Scenario UP, the value increases by 138.1% in Scenario PP, which is attributed to dam1. Likewise, dam 2 in the transitional area effectively reduces sediment loss, which is reflected by a 52.5% increase in *Ca*. Furthermore, the mitigation measures in Scenario PP with vegetation revetment and levees in Scenario EP act best. The conservation ability in the source area increased by 161.9% due to the dam retainment and vegetation revetment, and the levees helped increase the *Ca* by 3.49% in the deposit area.

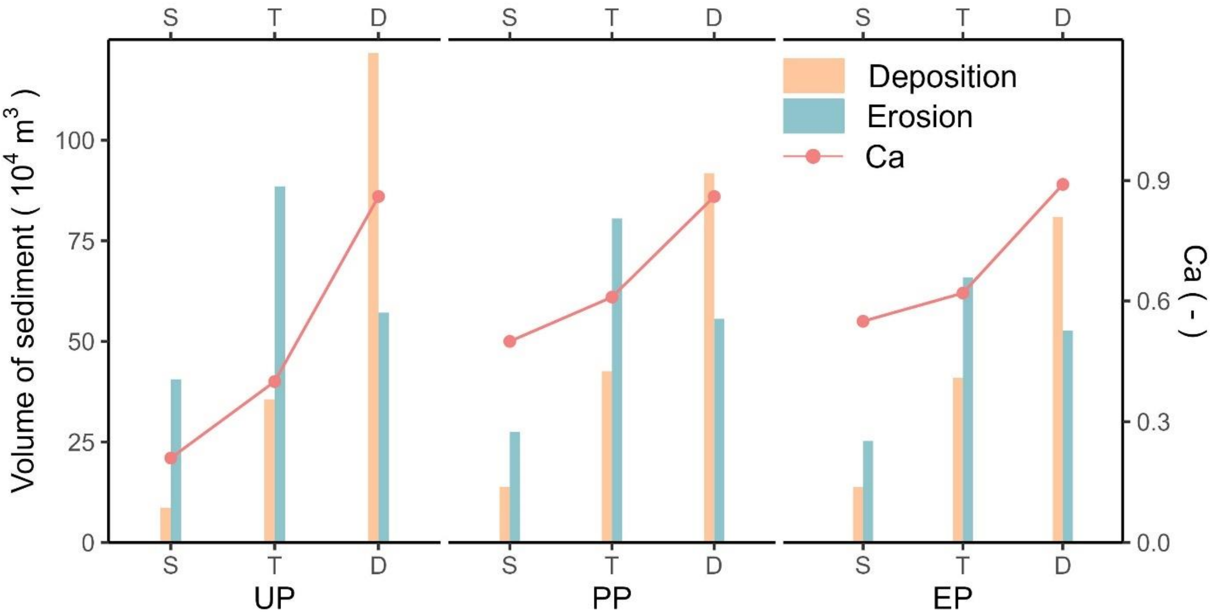

Figure 9: The volumes of sediment and the conservation ability (*Ca*) in the three areas for each scenario (S: source area; T: transitional area; D: deposit area).

The cumulative sediment yield time series for each scenario and the relative efficiency of scenarios UP and EP are presented in Fig. 10b and Fig. 10a, respectively. The steep curve of the output cumulative sediment indicates a significant increase in the deposition. Three increasing stages are consistent with the rainfall intensity in the three monsoons (May-Sept). The total sediment output in UP is the largest at ~30.4×10^4 m^3 followed by the sediment yield of PP at 26.3×10^4 m^3, and EP produced the least material at 19.3×10^4 m^3.

The relative efficiency over the period of controlling measures by human intervention in PP and EP (Fig. 10a) indicates three distinct stages. Stage I shows that the intervention measures in both scenarios completely prevent sediment transport. Later stage II shows a peculiar period when the effect of enhanced protective measures in EP pales in comparison with that in PP through repeated experiments. For stage III, the relative efficiency of the intervention measures in EP is greater than that in UP, which achieves the long-term effect and stable conservation of solid material.

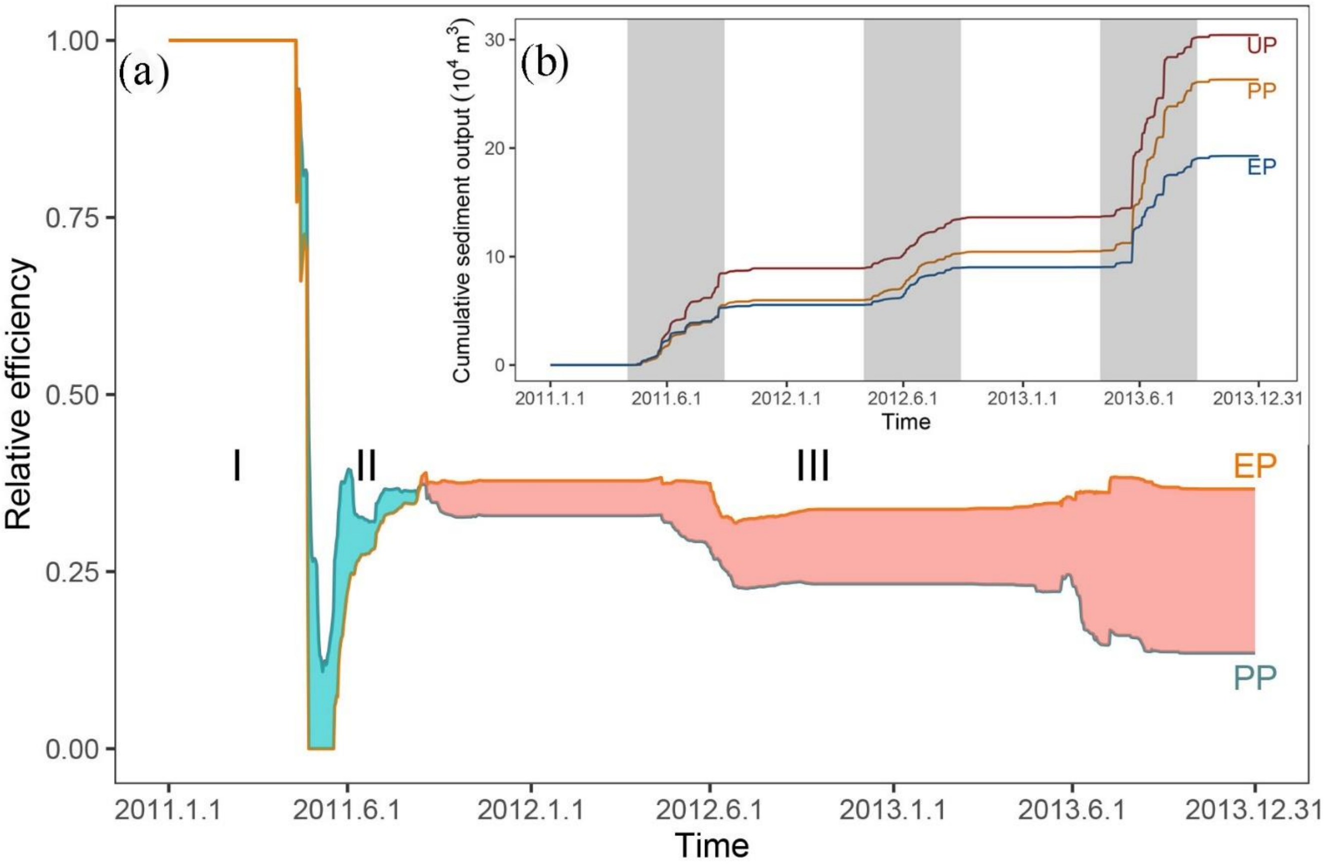

Figure 10: (a) Relative efficiency of Scenarios UP and EP compared with the UP (cyan shading represents when PP is more effective than EP and red shading represents the opposite); (b) Cumulative sediment yield over time (grey region highlighting three monsoons).

5. Discussion

5.1 Model calibration and uncertainty

Calibration and uncertainty are essential issues in the CAESAR-Lisflood (C-L) simulation of the geomorphic response to intervention measures based on the CA framework (Yeh and Li, 2006). A preliminary calibration was carried out by reproducing the geomorphic changes and water depth driven by an extreme rainfall event that occurred in 2018. The results (Fig. S3) demonstrated that the C-L model successfully replicated the flash flood event using the initial conditions and model parameters. And the calibration of the geomorphic response to the intervention measures was derived from a direct comparison between the model results and direct measurements (Fig. 4 and Fig. 5). As a result, the simulated water discharge was more than the measured discharge but with the same order of magnitude. Moreover, the errors of erosion and deposition depth between the simulation in Scenario PP and photographic evidence at three locations were less than 20%. The results suggest the robustness of the model settings and parameterisation.

The source of uncertainty is mainly from the model parameters and driving factors. Skinner et al. (2018b) provided a detailed sensitivity analysis of C-L, indicating that the sediment transport formula significantly influences a smaller catchment modelled by 10 m grid cells. The sediment transport law and the Wilcock and Crowe equations (Wilcock et al., 2003) have been proven suitable in the Xingping valley (Xie et al., 2018, 2022a, b; Li et al., 2020). Nevertheless, the empirical models of sediment transport overpredict bedload transport rates in steep streams (gradients greater than 3%) (D’Agostino and Lenzi, 1999; Yager et al., 2012). Additionally, the driving factor, the input hourly rainfall data downscaled from the daily sequence, is an unrealistic situation. Various sediment transport equations and downscaled hourly rainfall data need to be tested in the C-L model to further decrease uncertainty.

5.2 The intervention effects

In this study, more facilities create more comprehensive intervention systems which aim to control sediment delivery. The C-L model simulated the geomorphic responses to intervention measures and suggested the considerable influence of intervention measures on spatial modifications and sediment yield. The intervention measures lead to fewer total affected areas (7.9%-19.7%) and lower sediment yields (16.7%-36.7%), which are suggested in the overall evidence (see Fig. 6 and Fig. 10). The model's prediction of the overall catchment-scale dynamics due to extreme events is in line with the viewpoints of other authors (Chen et al., 2023; Lan et al., 2020; Chen et al., 2015).

The mitigation measures considerably change the soil conservation ability in the three subregions, especially in the source area. We hypothesise that the two main reasons for the decreased erosion in the source area compared to the other two subregions can be inferred from the interactions of loose material and topographic constraints. First, the abundant loose solid material formed by the strong earthquake has stabilised overall since the 2008 debris flow (details in Table S1). Second, the long and deep gullies are mainly located in the transitional area (Yaogouli, Shicouzi, Yangjiashan) and deposit area (Qinggangping), which provide more sediment supply than the source area. As shown in Fig. S4, the movement of the material occurs mainly in the branch valleys in the transitional and deposit zones.

Moreover, morphological details and the conservation ability of the three scenarios show the unique role played by different intervention measures. For example, check dams are most effective in blocking sediment, and vegetation revetments strengthen the conservation ability. The synergetic effect of the soil conservation ability increases by more than two-fold due to the combination of the check dams and the vegetation coverage. The levees are barriers with a discernable impact on sediment conservation but with specific object-oriented protection.

The effectiveness of mitigation measures decreases over time with a smaller downward trend. We supplemented a ten-year experiment to reveal the declining trend over an extended period. We randomly selected one of the 50 repeated rainfall datasets (year 2016-year 2025) downscaled by Li et al., 2020, which were generated from the NEX-GDDP product (spatial resolution: 0.25°×0.25°, temporal resolution: daily) under the RCP 4.5 emission scenario. The extracted rainfall sequence was then input into the C-L model to simulate the effectiveness of the three intervention scenarios. The result (Fig. 11) illustrates that stage III (the stable stage that started on the 161st day, in which Scenario EP's intervention measures were more effective) lasted longer than stages I and II. The relative effectiveness in both the PP and EP scenarios decreased gradually, while the curve fell faster in the PP scenario (slope: -1.65×10^{-5}) than in the EP scenario (slope: -1.31×10^{-5}).

The storage capacity of the checking dams fades with the sediment accumulated, which necessarily leads to a gradual decrease in intervention effectiveness. Additionally, vegetation revetments remain operationally effective in reducing sediment transport by stabilising topsoil over the period when the role of dam reservoirs gradually fails due to the lack of dredging work. Therefore, the vegetation protection strategy is vital for "green development" to reduce sediment loss but requires further efforts.

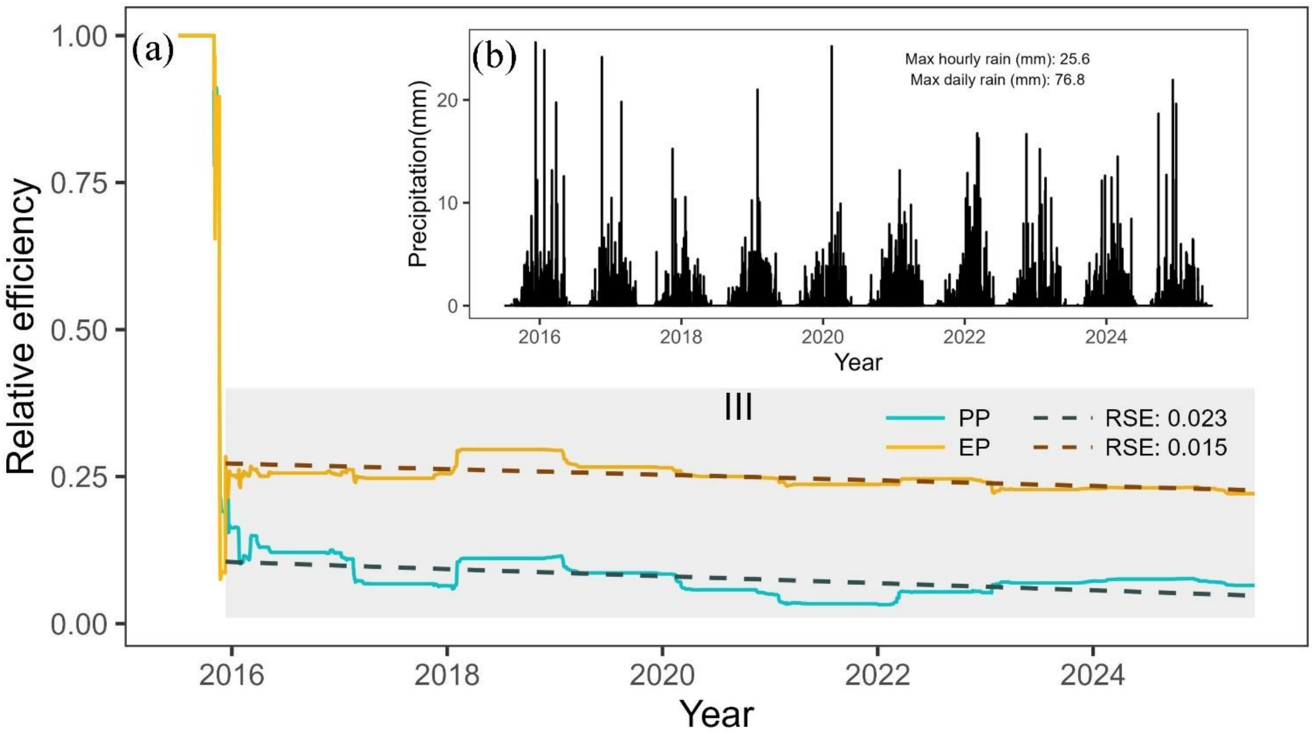

Figure 11: Rainfall input of ten years and relative efficiency of sediment intervention measures. (a) Relative efficiency changes over ten years (the grey region highlighting stage III, and the dashed lines indicate the linear fitting curves); (b) Rainfall downscaled from NEX-GDDP (NASA Earth Exchange Global Daily Downscaled Projections) product.

5.3 Limitations and applications

We built the dams and levees in our simulations by increasing the elevation in the expected location and assuming that it could not be eroded (see https://sourceforge.net/projects/caesar-lisflood/). This method proved experimentally feasible (Poeppl et al., 2019; Gioia and Schiattarella, 2020). The rigid dam and levee body embedded in the model were not broken or weakened over time so that the simulation result could underestimate the geohazard risk. Considering the complexity of the geo-hazard mechanism, the abovementioned tools cannot simulate the occurrence process of geo-hazard chain links. They ignore the possible instantaneous damage to the environment and facilities downstream. Some typical geohazard chains have focused on specified events in the short term and recreated the hazard lifecycle using physical and mechanical models (Fan et al., 2020).

The methods applied in the study further demonstrate that the C-L model is an effective tool for understanding short- to medium-term or long-term geomorphological changes (Ramirez et al., 2022; Li et al., 2020; Coulthard et al., 2012a) and observing the effectiveness of natural hazard intervention measures under different rainfall patterns. Our simulations indicate that the mitigation facilities in this study are effective, especially engineering efforts incorporating vegetation revetments in the upstream area, which would help decision-makers optimise the management strategies to control mountain disasters. Geotechnical engineering has disadvantages, even though it is a mature technology that identifies and fixes problems quickly (Cui and Lin, 2013), such as the need for extensive labour and expense and the difficulty of maintenance. While "green development", the planting and maintenance of vegetation cover can effectively prevent erosion by strengthening topsoil and absorbing excess rainwater via roots (Reichenbach et al., 2014; Stokes et al., 2014; Forbes and Broadhead, 2013; Mickovski et al., 2007). Alternatively, these methods can be used to study tree planting patterns on different slopes.

6. Conclusions

In this study, scenarios involving check dams, biological measures and artificial barriers were simulated using the C-L model to outline the erosion and deposition area, measure the impacts of blocking sediment, and examine how vegetation revetments help stabilise slopes. Four key findings are concluded. First, the engineering measures used for controlling sediment transport are efficient, and the performance in protecting the fragile environment can be improved by combining these engineering efforts with other intervention measures, such as vegetation revetments and artificial barriers. Second, the effectiveness of mitigation measures decreases over time. Third, the characteristics of the sediment transport patterns alter considerably due to the intervention measures. The stabilising sediment ability in the source area increased by 161.9% with the additional effect of vegetation revetments. Finally, the present intervention measures need to be revised to reduce erosion and should be combined with dredging work.

Declaration of interest statement

The authors declare that they have no known competing financial interests or personal relationships that could have appeared to influence the work reported in this paper.

Author contribution

Di Wang: Conceptualisation, Methodology, Software, Writing-original draft preparation. Ming Wang Kai Liu and Jun Xie: Supervision, Methodology, Writing- Reviewing and Editing, Validation.

Acknowledgements

This research was supported by the National Key Research and Development Plan (2017YFC1502902). The financial support is highly appreciated. The authors would also like to thank Professor Tom Coulthard and his team for their excellent work on the freely available C-L model (https://sourceforge.net/projects/caesar-lisflood).

Reference

Bates, P. D., Horritt, M. S., and Fewtrell, T. J.: A simple inertial formulation of the shallow water equations for efficient two-dimensional flood inundation modelling, J. Hydrol., 387, 33–45, https://doi.org/10.1016/j.jhydrol.2010.03.027, 2010.

Batty, M. and Xie, Y.: Possible urban automata, Environ. Plan. B Plan. Des., 24, 175–192, https://doi.org/10.1068/b240175, 1997.

Beven, K.: Linking parameters across scales: subgrid parameterizations and scale dependent hydrological models, Hydrol. Process., 9, 507–525, https://doi.org/https://doi.org/10.1002/hyp.3360090504, 1995.

Beven, K.: TOPMODEL:A critical, Hydrol. Process., 11, 1069–1085, https://doi.org/https://doi.org/10.1002/(SICI)1099-1085(199707)11:9<1069::AID-HYP545>3.0.CO;2-O, 1997.

Beven, K. J. and Kirkby, M. J.: A physically based, variable contributing area model of basin hydrology, Hydrol. Sci. Bull., 24, 43–69, https://doi.org/10.1080/02626667909491834, 1979.

Chen, N., Zhou, H., Yang, L., Yang, L., and Lv, L.: Analysis of benefits of debris flow control projects in southwest mountains areas of China, J. Chengdu Univ. Technol. (Science Technol. Ed., 40, 50–58, https://doi.org/10.3969/j.issn.1671-9727.2013.01.008, 2013.

Chen, X., Li, Z., Cui, P., and Liu, X.: Estimation of soil erosion caused by the 5.12 Wenchuan Earthquake, J. Mt. Sci., 27, 122–127, 2009.

Chen, X., Cui, P., You, Y., Chen, J., and Li, D.: Engineering measures for debris flow hazard mitigation in the Wenchuan earthquake area, Eng. Geol., 194, 73–85, https://doi.org/10.1016/j.enggeo.2014.10.002, 2015.

Chen, Y., Li, J., Jiao, J., Wang, N., Bai, L., Chen, T., Zhao, C., Zhang, Z., Xu, Q., and Han, J.: Modeling the impacts of fully-filled check dams on flood processes using CAESAR-lisflood model in the Shejiagou catchment of the Loess Plateau, China, J. Hydrol. Reg. Stud., 45, 101290, https://doi.org/10.1016/j.ejrh.2022.101290, 2023.

Cong, K., Li, R., and Bi, Y.: Benefit evaluation of debris flow control engineering based on the FLO-2D model, Northwest. Geol., 52, https://doi.org/10.19751/j.cnki.61-1149/p.2019.03.019, 2019.

Couclelis, H.: From cellular automata to urban models: new principles for model development and implementation, Environ. Plan. B Plan. Des., 24, 165–174, https://doi.org/10.1068/b240165, 1997.

Coulthard, T. J. and Skinner, C. J.: The sensitivity of landscape evolution models to spatial and temporal rainfall resolution, Earth Surf. Dyn., 4, 757–771, https://doi.org/10.5194/esurf-4-757-2016, 2016.

Coulthard, T. J. and Wiel, Van De J., M.: Modelling long term basin scale sediment connectivity, driven by spatial land use changes, Geomorphology, 277, 265–281, https://doi.org/10.1016/j.geomorph.2016.05.027, 2017.

Coulthard, T. J., Macklin, M. G., and Kirkby, M. J.: A cellular model of Holocene upland river basin and alluvial fan evolution, Earth Surf. Process. Landforms, 27, 269–288, https://doi.org/10.1002/esp.318, 2002.

Coulthard, T. J., Hancock, G. R., and Lowry, J. B. C.: Modelling soil erosion with a downscaled landscape evolution model, Earth Surf. Process. Landforms, 37, 1046–1055, https://doi.org/10.1002/esp.3226, 2012a.

Coulthard, T. J., Ramirez, J., Fowler, H. J., and Glenis, V.: Using the UKCP09 probabilistic scenarios to model the amplified impact of climate change on drainage basin sediment yield, Hydrol. Earth Syst. Sci., 16, 4401–4416, https://doi.org/10.5194/hess-16-4401-2012, 2012b.

Coulthard, T. J., Neal, J. C., Bates, P. D., Ramirez, J., de Almeida, G. A. M., and Hancock, G. R.: Integrating the LISFLOOD-FP 2D hydrodynamic model with the CAESAR model: Implications for modelling landscape evolution, Earth Surf. Process. Landforms, 38, 1897–1906, https://doi.org/10.1002/esp.3478, 2013.

Cui, P. and Lin, Y.: Debris-Flow Treatment: The Integration of Botanical and Geotechnical Methods, J. Resour. Ecol., 4, 097–104, https://doi.org/10.5814/j.issn.1674-764x.2013.02.001, 2013.

Cui, P., Zhou, G. G. D., Zhu, X. H., and Zhang, J. Q.: Scale amplification of natural debris flows caused by cascading landslide dam failures, Geomorphology, 182, 173–189, https://doi.org/10.1016/j.geomorph.2012.11.009, 2013.

D'Agostino, V. and Lenzi, M. A.: Bedload transport in the instrumented catchment of the Rio Cordon. Part II: Analysis of the bedload rate, Catena, 36, 191–204, https://doi.org/10.1016/S0341-8162(99)00017-X, 1999.

Einstein, H. A.: The Bed-Load Function for Sediment Transportation in Open Channel Flows, 1950.

Fan, X., Yang, F., Siva Subramanian, S., Xu, Q., Feng, Z., Mavrouli, O., Peng, M., Ouyang, C., Jansen, J. D., and Huang, R.: Prediction of a multi-hazard chain by an integrated numerical simulation approach: the Baige landslide, Jinsha River, China, Landslides, 17, 147–164, https://doi.org/10.1007/s10346-019-01313-5, 2020.

Feng, W., He, S., Liu, Z., Yi, X., and Bai, H.: Features of Debris Flows and Their Engineering Control Effects at Xinping Gully of Pingwu County, J. Eng. Geol., 25, https://doi.org/10．13544 / j．cnki．jeg．2017．03．027, 2017.

Forbes, K. and Broadhead, J.: Forests and landslides: the role of trees and forests in the prevention of landslides and rehabilitation of landslide-affected areas in Asia, FAO, 14–18 pp., 2013.

Gioia, D. and Schiattarella, M.: Modeling Short-Term Landscape Modification and Sedimentary Budget Induced by Dam Removal: Insights from LEM Application, Appl. Sci., 10, 7697, https://doi.org/10.3390/app10217697, 2020.

Goldberg, D. E.: Genetic Algorithms in Search, Optimization, and Machine Learning, Addison-Wesley Longman Publishing Co., Inc., 372 pp., https://doi.org/10.1007/BF01920603, 1989.

Gorum, T., Fan, X., van Westen, C. J., Huang, R. Q., Xu, Q., Tang, C., and Wang, G.: Distribution pattern of earthquake-induced landslides triggered by the 12 May 2008 Wenchuan earthquake, Geomorphology, 133, 152–167, https://doi.org/10.1016/j.geomorph.2010.12.030, 2011.

Guo, Q., Xiao, J., and Guan, X.: The characteristics of debris flow activities and its optimal timing for the control in Shikan River Basin Pingwu Country, Chinese J. Geol. Hazard Control, 29, https://doi.org/10. 16031/j. cnki. issn. 1003-8035. 2018. 03. 05, 2018.

Hancock, G. R., Verdon-Kidd, D., and Lowry, J. B. C.: Soil erosion predictions from a landscape evolution model – An assessment of a post-mining landform using spatial climate change analogues, Sci. Total Environ., 601–602, 109–121, https://doi.org/10.1016/j.scitotenv.2017.04.038, 2017.

He, J., Zhang, L., Fan, R., Zhou, S., Luo, H., and Peng, D.: Evaluating effectiveness of mitigation measures for large debris flows in Wenchuan, China, Landslides, 19, 913–928, https://doi.org/10.1007/s10346-021-01809-z, 2022.

Huang, R.: Geohazard assessment of the Wenchuan earthquake, Science Press, Beijing, 944 pp., 2009.

Huang, R. and Fan, X.: The landslide story, Nat. Geosci., 6, 325–326, https://doi.org/10.1038/ngeo1806, 2013.

J.B.C. Lowry, M. Narayan, G.R. Hancock, and K.G. Evans: Understanding post-mining landforms:Utilising pre-mine geomorphology to improve rehabilitation outcomes, Geomorphology, 328, 93–107, https://doi.org/10.1016/j.geomorph.2018.11.027, 2019.

Lan, H., Wang, D., He, S., Fang, Y., Chen, W., Zhao, P., and Qi, Y.: Experimental study on the effects of tree planting on slope stability, Landslides, 17, 1021–1035, https://doi.org/10.1007/s10346-020-01348-z, 2020.

Lee, T. and Jeong, C.: Nonparametric statistical temporal downscaling of daily precipitation to hourly precipitation and implications for climate change scenarios, J. Hydrol., 510, 182–196, https://doi.org/10.1016/j.jhydrol.2013.12.027, 2014.

Li, C., Wang, M., and Liu, K.: A decadal evolution of landslides and debris flows after the Wenchuan earthquake, Geomorphology, 323, 1–12, https://doi.org/10.1016/j.geomorph.2018.09.010, 2018.

Li, C., Wang, M., Liu, K., and Coulthard, T. J.: Landscape evolution of the Wenchuan earthquake-stricken area in response to future climate change, J. Hydrol., 590, 125244, https://doi.org/10.1016/j.jhydrol.2020.125244, 2020.

Marchi, L., Comiti, F., Crema, S., and Cavalli, M.: Channel control works and sediment connectivity in the European Alps, Sci. Total Environ., 668, 389–399, https://doi.org/10.1016/j.scitotenv.2019.02.416, 2019.

Mickovski, S. B., Bengough, A. G., Bransby, M. F., Davies, M. C. R., Hallett, P. D., and Sonnenberg, R.: Material stiffness, branching pattern and soil matric potential affect the pullout resistance of model root systems, Eur. J. Soil Sci., 58, 1471–1481, https://doi.org/10.1111/j.1365-2389.2007.00953.x, 2007.

Poeppl, R. E., Coulthard, T., Keesstra, S. D., and Keiler, M.: Modeling the impact of dam removal on channel evolution and sediment delivery in a multiple dam setting, Int. J. Sediment Res., 34, 537–549, https://doi.org/10.1016/j.ijsrc.2019.06.001, 2019.

Ramirez, J. A., Zischg, A. P., Schürmann, S., Zimmermann, M., Weingartner, R., Coulthard, T., and Keiler, M.: Modeling the geomorphic response to early river engineering works using CAESAR-Lisflood, Anthropocene, 32, https://doi.org/10.1016/j.ancene.2020.100266, 2020.

Ramirez, J. A., Mertin, M., Peleg, N., Horton, P., Skinner, C., Zimmermann, M., and Keiler, M.: Modelling the long-term geomorphic response to check dam failures in an alpine channel with CAESAR-Lisflood, Int. J. Sediment Res., 37, 687–700, https://doi.org/10.1016/j.ijsrc.2022.04.005, 2022.

Reichenbach, P., Busca, C., Mondini, A. C., and Rossi, M.: The Influence of Land Use Change on Landslide Susceptibility Zonation: The Briga Catchment Test Site (Messina, Italy), Environ. Manage., 54, 1372–1384, https://doi.org/10.1007/s00267-014-0357-0, 2014.

Saynor, M. J., Lowry, J. B. C., and Boyden, J. M.: Assessment of rip lines using CAESAR-Lisflood on a trial landform at the Ranger Uranium Mine, L. Degrad. Dev., 30, 504–514, https://doi.org/10.1002/ldr.3242, 2019.

Skinner, C. J., Coulthard, T. J., Schwanghart, W., Van De Wiel, M. J., and Hancock, G.: Global sensitivity analysis of parameter uncertainty in landscape evolution models, Geosci. Model Dev., 11, 4873–4888, https://doi.org/10.5194/gmd-11-4873-2018, 2018a.

Skinner, C. J., Coulthard, T. J., Schwanghart, W., Van De Wiel, M. J., and Hancock, G.: Global sensitivity analysis of parameter uncertainty in landscape evolution models, Geosci. Model Dev., 11, 4873–4888, https://doi.org/10.5194/gmd-11-4873-2018, 2018b.

Slingerland, N., Beier, N., and Wilson, G.: Stress testing geomorphic and traditional tailings dam designs for closure using a landscape evolution model, in: Proceedings of the 13th International Conference on Mine Closure, 1533–1544, https://doi.org/10.36487/ACG_rep/1915_120_Slingerland, 2019.

Stokes, A., Douglas, G. B., Fourcaud, T., Giadrossich, F., Gillies, C., Hubble, T., Kim, J. H., Loades, K. W., Mao, Z., McIvor, I. R., Mickovski, S. B., Mitchell, S., Osman, N., Phillips, C., Poesen, J., Polster, D., Preti, F., Raymond, P., Rey, F., Schwarz, M., and Walker, L. R.: Ecological mitigation of hillslope instability: Ten key issues facing researchers and practitioners, Plant Soil, 377, 1–23, https://doi.org/10.1007/s11104-014-2044-6, 2014.

Thomson, H. and Chandler, L.: Tailings storage facility landform evolution modelling, in: Proceedings of the 13th International Conference on Mine Closure, 385–396, https://doi.org/10.36487/ACG_rep/1915_31_Thomson, 2019.

Wang, M., Yang, W., Shi, P., Xu, C., and Liu, L.: Diagnosis of vegetation recovery in mountainous regions after the wenchuan earthquake, IEEE J. Sel. Top. Appl. Earth Obs. Remote Sens., 7, 3029–3037, https://doi.org/10.1109/JSTARS.2014.2327794, 2014a.

Wang, M., Liu, M., Yang, S., and Shi, P.: Incorporating Triggering and Environmental Factors in the Analysis of Earthquake-Induced Landslide Hazards, Int. J. Disaster Risk Sci., 5, 125–135, https://doi.org/10.1007/s13753-014-0020-7, 2014b.

Wang, N., Han, B., Pang, Q., and Yu, Z.: post-evaluation model on effectiveness of debris flow control, J. Eng. Geol., 23, 219–226, https://doi.org/10.13544/j.cnki.jeg.2015.02.005, 2015.

Van De Wiel, M. J., Coulthard, T. J., Macklin, M. G., and Lewin, J.: Embedding reach-scale fluvial dynamics within the CAESAR cellular automaton landscape evolution model, Geomorphology, 90, 283–301, https://doi.org/10.1016/j.geomorph.2006.10.024, 2007.

Wilcock, P. R., Asce, M., and Crowe, J. C.: Surface-based Transport Model for Mixed-Size Sediment Surface-based Transport Model for Mixed-Size Sediment, 9429, https://doi.org/10.1061/(ASCE)0733-9429(2003)129, 2003.

Xie, J., Wang, M., Liu, K., and Coulthard, T. J.: Modeling sediment movement and channel response to rainfall variability after a major earthquake, Geomorphology, 320, 18–32, https://doi.org/10.1016/j.geomorph.2018.07.022, 2018.

Xie, J., Coulthard, T. J., and McLelland, S. J.: Modelling the impact of seismic triggered landslide location on basin sediment yield, dynamics and connectivity, Geomorphology, 398, 108029, https://doi.org/10.1016/j.geomorph.2021.108029, 2022a.

Xie, J., Coulthard, T. J., Wang, M., and Wu, J.: Tracing seismic landslide-derived sediment dynamics in response to climate change, Catena, 217, 106495, https://doi.org/10.1016/j.catena.2022.106495, 2022b.

Xu, C., Xu, X., Yao, X., and Dai, F.: Three (nearly) complete inventories of landslides triggered by the May 12, 2008 Wenchuan Mw 7.9 earthquake of China and their spatial distribution statistical analysis, Landslides, 11, 441–461, https://doi.org/10.1007/s10346-013-0404-6, 2014.

Yager, E. M., Turowski, J. M., Rickenman, D., and McArdell, B. W.: Sediment supply, grain protrusion, and bedload transport in mountain streams, Geophys. Res. Lett., 39, 1–5, https://doi.org/10.1029/2012GL051654, 2012.

Yang, Z., Duan, X., Huang, J., Dong, Y., Zhang, X., Liu, J., and Yang, C.: Tracking long-term cascade check dam siltation: implications for debris flow control and landslide stability, Landslides, 18, 3923–3935, https://doi.org/10.1007/s10346-021-01755-w, 2021.

Yeh, A. G. O. and Li, X.: Errors and uncertainties in urban cellular automata, Comput. Environ. Urban Syst., 30, 10–28, https://doi.org/10.1016/j.compenvurbsys.2004.05.007, 2006.

Yu, B., Yang, Y., Su, Y., Huang, W., and Wang, G.: Research on the giant debris flow hazards in Zhouqu County, Gansu Province on August 7, 2010, J. Eng. Geol., 18, 437–444, https://doi.org/10.3969/j.issn.1004-9665.2010.04.001, 2010.

Zhang, L. and Liang, K.: Research on economic benefit evaluation of the prevention and cure project for debris flow, Chinese J. Geol. Hazard Control, 16, 48–53, https://doi.org/10.3969/j.issn.1003-8035.2005.03.011, 2005.

Zhang, X., Wang, M., Liu, K., Xie, J., and Xu, H.: Using NDVI time series to diagnose vegetation recovery after major earthquake based on dynamic time warping and lower bound distance, Ecol. Indic., 94, 52–61, https://doi.org/10.1016/j.ecolind.2018.06.026, 2018.

Zhou, H., Chen, N., Lu, Y., and Li, B.: Control Effectiveness of Check Dams in Debris Flow Gully: A Case of Huashiban Gully in Earthquake Worst-stricken Area，Beichuan County, J. Mt. Sci., 30, 347–354, https://doi.org/10.3969/j.issn.1008-2786.2012.03.015, 2012.